Design Optimization, Cabling and Stability of Large-Diameter High J_c Nb_3Sn Wires

S. C. Hopkins, B. Medina-Clavijo, C. Barth, J. Fleiter, and A. Ballarino

(Invited Paper)

***Abstract*—In the framework of the High Field Magnets (HFM) program, CERN is developing and qualifying Nb_3Sn Rutherford cables to support magnet development towards the requirements of a future energy-frontier collider, using both state-of-the-art commercial wires and experimental wires under development with industrial partners. The trend towards higher current density and larger diameter wires imposes challenges for magneto-thermal stability. In this study, rolling trials and Rutherford cabling have been performed at CERN for two designs of a 1 mm diameter distributed tin Nb_3Sn wire produced by KAT, and for 1 mm and 1.1 mm diameter RRP® Nb_3Sn wires procured from Bruker OST, and the self-field stability and cabling degradation have been analyzed. The 1 mm RRP® wire shows significant degradation in I_c and stability on cabling. Although the latter is not expected to impact the performance of research magnets, the potential of heat treatment optimization to improve stability has also been quantified. The distributed tin wire shows substantially poorer stability, but promising indications of low cabling degradation. The influence of wire design characteristics on cabling behavior and stability have been assessed, and the implications for future wire optimization towards high field accelerator magnet applications have been discussed.**

***Index Terms*—Niobium-tin, multifilamentary superconductors, heat treatment, critical current density.**

I. Introduction

In THE context of the High Field Magnets (HFM) program, CERN is procuring Nb_3Sn wire and developing Rutherford cables to support two objectives for magnet development, both internally [1] and in collaborations [2], [3]: firstly, demonstrating a robust technology for 12 T Nb_3Sn accelerator magnets, and secondly, developing ultimate performance Nb_3Sn dipole magnets targeting 14 T and above. The latter goal will also require development of wire beyond the present state of the art towards the non-copper critical current density (J_c) target of 1500 A mm^{-2} at 16 T and 4.2 K set for the proposed FCC-hh hadron collider [1], [4], supported by academic and industrial wire development collaborations.

High field magnet designs often favor wide cables of large-diameter wire, combining high engineering current density (J_e) with a manageable inductance; but these designs are also more challenging for mechanical stability of cables during winding and for magneto-thermal stability. Magneto-thermal instabilities can result in quenches at currents significantly below the critical current, thereby limiting the performance of a coil. Flux jumps arise from a rapid redistribution of current, and can be attributed to self-field instability (originating from transport current, e.g., during current ramps) or to magnetization instability (originating from persistent currents) [5], [6].

Magnetization instability is controlled primarily by dividing the superconductor into small twisted filaments, i.e., with a low effective diameter (d_{eff}). If d_{eff} is not sufficiently small to render the filaments adiabatically stable, stable operation depends on dynamic stability, which is enhanced by high conductivity of the copper stabilizer [5]. Magnetization instability, if present, becomes significant at low fields [6].

As filament twisting is ineffective against the self-field of a multifilamentary composite [5], the adiabatic self-field stability criterion depends on the overall wire diameter and J_c. Self-field stability is often the factor limiting magnet performance in the intermediate field region [6], and again this can be addressed by enhancing dynamic stability [5].

In this article, cabling degradation and magneto-thermal stability are evaluated for two categories of Nb_3Sn internal tin wire with diameters of 1 mm and above: Bruker Restacked Rod Process (RRP®) wire procured commercially, and a distributed tin wire produced by Kiswire Advanced Technology (KAT) in the context of a collaboration with CERN. These are compared with the extensively characterized RRP® wires procured for the High-Luminosity LHC (HL-LHC) project magnets, with diameters of 0.7 mm and 0.85 mm, and considered against the requirements of the planned applications. The potential for heat treatment optimization to improve the self-field stability is investigated, with reference to microscopy data and the effects on RRR and I_c; and the consequences for the future selection and development of distributed barrier and distributed tin wire tapes are discussed.

II. Conductors

A. Wire Types

Two categories of internal tin wire are considered in this study: distributed barrier, exemplified by Restacked Rod Process (RRP®) wire produced by Bruker, and distributed tin,

Manuscript received 13 November 2022; revised 20 January 2023; accepted 26 January 2023. Date of publication 27 March 2023; date of current version 30 March 2023. *(Corresponding author: S. C. Hopkins.)*

The authors are with the European Organization for Nuclear Research (CERN), 1211 Geneva, Switzerland (e-mail: simon.hopkins@cern.ch).

Color versions of one or more figures in this article are available at https://doi.org/10.1109/TASC.2023.3254497.

Digital Object Identifier 10.1109/TASC.2023.3254497

This work is licensed under a Creative Commons Attribution 4.0 License. For more information, see https://creativecommons.org/licenses/by/4.0/

TABLE I
CHARACTERISTICS OF THE BRUKER RRP® WIRES

Property	HL-LHC		HFM	
	11 T	MQXF	ERMC-1	DEM-1.1
Diameter (mm)	0.7	0.85	1.0	1.1
RRP® Layout	108/127		162/169	
d_s (µm) [a]	45	55	58	64
Cu/non-Cu [b]	1.15 ± 0.1	1.2 ± 0.1	0.9 ± 0.2	0.9 ± 0.2
Nb:Sn	3.6 (reduced Sn)		3.4 (standard Sn)	
Standard heat treatment [c]	650 °C 50 h	665 °C 50 h	650 °C 50 h	665 °C 50 h
RRR, round [d]	309 ± 35	345 ± 40	290 ± 33	266 ± 39
RRR, rolled [d]	174 ± 29	215 ± 29	206 ± 27	203 ± 36

[a] Geometrical sub-element diameter
[b] Range of Cu/non-Cu permitted by specification
[c] Final plateau of the manufacturer's final recommended heat treatment cycle; RRP® heat treatments begin with plateaus of 48 h at 210 °C and 48 h at 400 °C
[d] Residual resistivity ratio measured in CERN acceptance tests (mean ± standard deviation) after the standard heat treatment, for round wire and after rolling with a diameter reduction of 15 %

represented here by wires produced by Kiswire Advance Technology (KAT) for CERN collaboration agreement KE3449.

The characteristics of the RRP® wires are summarized in Table I. The study is focused on wires with a 162/169 architecture and diameters of 1.0 and 1.1 mm, referred to as 'ERMC-1' and 'DEM-1.1' respectively, which were procured for magnet development activities now forming part of the HFM project. The specifications of these wire types were designed to prioritize high current density (both J_c and J_e), as they were intended for use in research coils and model magnets for the development of future higher-field accelerator magnets. To that end, a low Cu/non-Cu ratio was specified, and the supplier was given a J_c target as well as a minimum I_c specification; and the J_c target was exceeded in production.

Large quantities of RRP® wire with a 108/127 layout and a Cu/non-Cu of ∼1.2 were procured, extensively characterized and cabled at CERN for the HL-LHC project, and these conductors serve as a baseline for comparison. The wires assigned to 11 T dipoles and Inner Triplet quadrupoles (MQXF) have diameters of 0.7 mm and 0.85 mm respectively. The HFM wires differ from these HL-LHC reference wires in several important respects: larger diameter, larger sub-element diameter, lower copper fraction, and a lower Nb:Sn ratio in the sub-elements (higher tin stoichiometry).

As shown in Fig. 1, the J_c of the ERMC-1 and DEM-1.1 wires significantly exceeds that of the HL-LHC reference wires, as intended. This is consistent with performance trends as a function of sub-element size and stoichiometry in the literature [7]. Despite the J_c-optimized design, with the recommended heat treatments the residual resistivity ratio (RRR) is high (see Table I): in particular, for wire rolled with a 15% diameter reduction, the mean RRR exceeds 200 (compared to a minimum specification of 100), intermediate between the values for the HL-LHC 11 T and MQXF wires.

The characteristics of the KAT distributed tin wires are summarized in Table II. The present study focuses on the most recent trial wire, identified as 'Task 5', but the characteristics of the

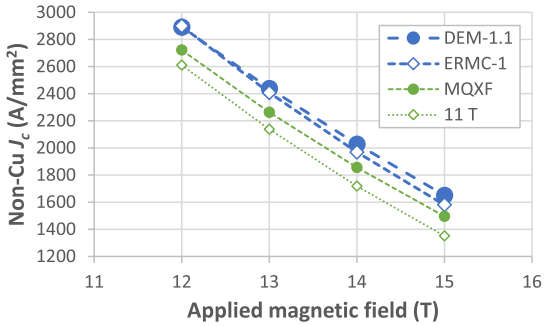

Fig. 1. Non-Cu J_c as a function of the applied magnetic field B for the four RRP® wire types at ∼4.3 K. The values plotted are the mean values of J_c for round (as-received) wire, calculated from the I_c measured during acceptance testing in liquid helium at CERN, without self-field or temperature corrections, and the measured Cu/non-Cu fraction.

TABLE II
CHARACTERISTICS OF THE KAT DISTRIBUTED TIN WIRES

Property	Task 4	Task 5
Year of production	2020	2021
Length delivered (km)	5	20
Mean piece length (m)	230	1432
Diameter (mm)	1.0	
Cu/non-Cu [a]	1.0 ± 0.1	
Layout	E199R192	
Number of modules	132 Nb, 60 Sn-Ti	138 Nb, 54 Sn-Ti
d_s (µm) [b]	45	55

[a] Range of Cu/non-Cu permitted by specification
[b] Geometrical Nb module diameter

TABLE III
CABLE DESIGNS

Property	MQXF	ERMC	FalconD	R2D2 HF
Wire type	MQXF	ERMC-1	ERMC-1, KAT	DEM-1.1
Strands, number × diameter (mm)	40 × 0.85	40 × 1.0	40 × 1.0	21 × 1.1
Cable pitch (mm)	109	120	110–120	84
Keystone	0.4 °	None	0.5 °	None
Core	Steel [a]	Steel [a]	Steel [a]	None
Mid-thickness (mm)	1.525	1.82	1.80	1.965

[a] Stainless steel 1.4404 (316L), 0.025 mm thick

previous iteration ('Task 4') are given for comparison. 'Module' refers to the constituent elements of the wire stack (either Nb filaments in a Cu matrix, or a Sn-Ti source).

The cross-sections of the wires are shown in Fig. 2.

B. Cable Designs and Magnet Applications

The wire types presented here will be used in several designs of Rutherford cable, with the nominal characteristics tabulated in Table III, according to the magnet application.

In the context of HFM, CERN is engaged in magnet development collaborations with several partners. The FalconD collaboration with INFN (Italy) is developing a cos-θ model dipole targeting a 12 T bore field [2], for which it is planned to use the

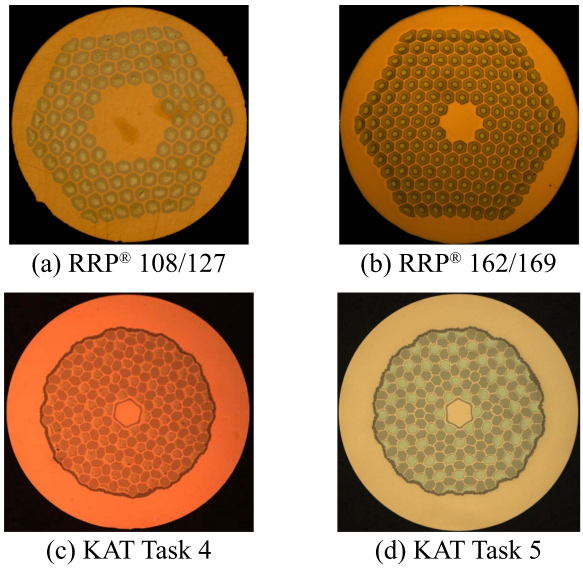

Fig. 2. Optical micrographs of the cross-sections of the wires under study: (a) RRP® 108/127: HL-LHC 11 T and MQXF wires (MQXF shown, 0.85 mm diameter), (b) RRP® 162/169: HFM ERMC-1 and DEM-1.1 wires (ERMC-1 shown), (c) KAT Task 4 wire and (d) KAT Task 5 wire.

ERMC-1 wire in a 40-strand cable with a keystone of 0.5°. The ERMC-1 wire will also be used in CERN's enhanced Racetrack Model Coil (eRMC) [8] program for R&D purposes, which requires a cable of similar dimensions but without keystoning. These cable designs are also used for testing the cabling behavior of R&D wire under consideration for future research coils: in the present case, the FalconD cable layout has been used for cabling trials of KAT wire.

Cable type 'R2D2 HF' in Table III refers to the high-field conductor for R2D2, a single-layer graded Research Racetrack Dipole Demonstrator magnet under development with CEA (France), as a first step to developing the technologies needed for a proposed single aperture block dipole demonstrator [3]. This is a cable with 21 DEM-1.1 strands, without keystone or core (and designed to match the width of the corresponding low-field cable with 0.7 mm diameter strands not presented here). The MQXF cable design for HL-LHC is included in Table III for comparison.

III. Samples and Methods

Critical current (I_c) and RRR measurements, and electron microscopy, were performed on samples after heat treatment under vacuum. Samples for measurement of I_c (and quench current) were wound on Ti-Al-V VAMAS barrels, reacted in a large tube furnace under vacuum, and measured on the same barrels. Samples for measurement of RRR and for microscopy were either reacted alongside the barrels, or encapsulated in quartz tubes under vacuum to allow reaction in a smaller research furnace. The research furnace is open to atmosphere and contains several tubes from which encapsulated samples can be ejected on a schedule, which allows the effects of different heat treatment durations to be compared.

Virgin/round wire samples are cut from the wire spool as received. Rolled samples are prepared by uniaxial rolling, to simulate the deformation induced by cabling (away from the cable edges), for which the rolling reduction is defined by the relative reduction in diameter: 15% unless otherwise specified. Extracted strands are strands removed from a cable after production. For evaluation of cabling degradation, wherever possible extracted strands are measured alongside virgin samples taken from an adjacent position on the wire spool.

Transport I_c and stability measurements were performed in an applied magnetic field of up to 15 T, and at temperatures of nominally 1.9 K (superfluid He-II) and 4.3 K (liquid helium). I_c is calculated using a 0.1 μV/cm criterion. Stability was evaluated from *V-I* measurements with a ramp rate of 12 A/s, which primarily test self-field stability [6]. Several current ramps were performed at each magnetic field, starting at 15 T and decreasing in small steps, and for each ramp the maximum current reached ($I_{\max}$) was recorded. In case of a quench, $I_{\max}$ corresponds to the quench current; if a stable transition to the normal state was observed, the corresponding I_c was also recorded. Unless otherwise specified, plots show the mean $I_{\max}$ (open symbols) and I_c (solid symbols) at each applied magnetic field, without adjustment for the sample self-field or temperature corrections, colored according to the measurement temperature (blue for 1.9 K, orange for 4.3 K).

Scanning electron microscopy (SEM) was performed using a Zeiss Evo 10 microscope on metallographic samples mounted in transverse cross-section. Image analysis of backscattered electron micrographs was performed using custom Python scripts and the scikit-image library for post-processing, segmentation and analysis. Reported areas represent the total area of the segmented phase in the wire cross-section. Barrier thicknesses were obtained using a minimum distance between the inner and outer periphery at each point around each sub-element barrier, and averaged over all sub-elements.

IV. Stability of MQXF Wire

As a baseline reference, stability tests were first performed for the MQXF conductor. Over the tested range (6–15 T and up to ~1900 A), no quenches occurred, and the $I_c(B)$ dependence was in good agreement with the $I_c(B)$ trend extrapolated from the average I_c measured during wire acceptance tests in the 12–15 T range (Fig. 3). For the tested samples, self-field stability therefore does not limit performance.

V. Stability and Cabling Degradation of ERMC-1

A. Stability Measurements for Standard Heat Treatments

A similar test was then performed for the ERMC-1 wire, and the results for virgin wire are presented in Fig. 4. At 4.3 K, complete normal state transitions from which I_c could be accurately determined were measured only at 11 T and above, but at lower fields the quench current remains approximately equal to the extrapolated I_c down to the lowest field tested (9 T). This corresponds to a current of ~2000 A, which is the maximum

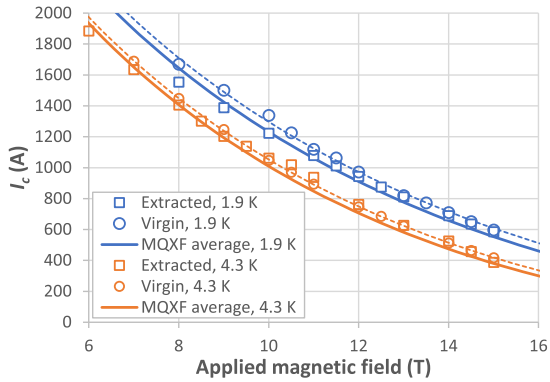

Fig. 3. Measured $I_c(B)$ at 4.3 K and 1.9 K for virgin MQXF wire and an extracted strand from an MQXF cable for the standard heat treatment (665 °C 50 h). Dashed lines show the extrapolated $I_c(B)$ for the virgin samples, and solid lines show the extrapolated average virgin MQXF wire $I_c(B)$ from wire acceptance tests for comparison. The tested virgin and extracted samples are from cabling at LBNL (reference P43OL1123AE27) of wire spool reference PO08S00343A01U. In this plot, open symbols have been used for I_c (for visibility of overlapping markers).

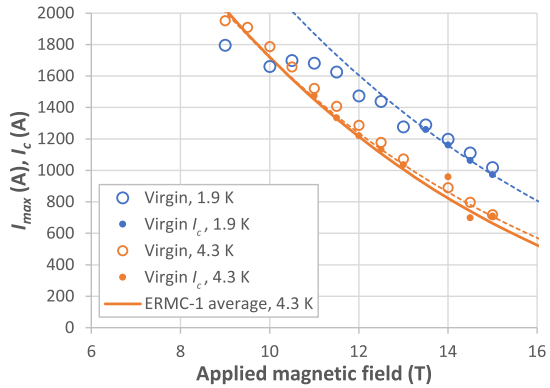

Fig. 4. Measured $I_{\max}(B)$ and $I_c(B)$ at 4.3 K and 1.9 K for virgin ERMC-1 wire after the standard heat treatment (650 °C 50 h). Dashed lines show the extrapolated $I_c(B)$ for the present samples; the solid line shows the extrapolated average virgin ERMC-1 wire $I_c(B)$ from wire acceptance tests at 4.3 K for comparison.

current that can be injected via the copper terminations of the VAMAS barrels. At 1.9 K, quench currents deviate appreciably below the extrapolated $I_c(B)$ curve at 13 T and below, and at 10 T and below the quench current is lower at 1.9 K than 4.3 K. The planned magnets are intended for operation at 1.9 K in order to take advantage of the maximum I_c, so such a crossover is of course undesirable: whether it constitutes a practical limitation must be assessed considering the load line and temperature margin of the application.

The corresponding results for an extracted strand from a trial cable of the FalconD design are shown in Fig. 5. In the high-field range for which I_c was measurable, the I_c is lower than that of the virgin wire, corresponding to some cabling degradation of I_c (the offset between markers and dashed lines in Fig. 5). The $I_{\max}(B)$ deviates from the extrapolation of this high-field behavior at 13 T and 14 T, for 4.3 K and 1.9 K

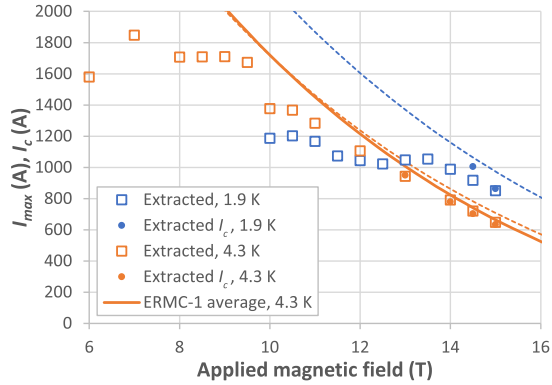

Fig. 5. Measured $I_{\max}(B)$ and $I_c(B)$ at 4.3 K and 1.9 K for an extracted ERMC-1 strand from a trial FalconD cable after the standard heat treatment (650 °C 50 h). The lines are virgin wire performance for comparison, as shown in Fig. 4.

respectively, with the intersection between the quench current curves for the two temperatures lying at 12.5 T. The stability of the FalconD extracted strand sample is therefore substantially degraded relative to the ERMC-1 virgin wire.

B. Heat Treatment Optimization

Having observed that stability limited the $I_c(B)$ performance for the ERMC-1 wire, especially after cabling in the FalconD design, a study was started to assess whether changes to the heat treatment would allow the achievable current to be increased.

Heat treatment optimization for Nb_3Sn wires typically focuses on adjusting the temperature and duration of the final plateau to achieve the preferred compromise between I_c and RRR. For ERMC-1, a 665 °C heat treatment had originally been planned and, following production experience, such an optimization concluded that a reduction to 650 °C was needed to ensure conformity with the RRR specification. Further decreasing the temperature or duration would be expected to increase RRR and decrease I_c [9], improving dynamic stability.

The wire design does, however, permit only a limited window for optimization. Literature data suggest that a reduction in temperature from 650 °C to 640 °C for similar RRP® wires (132/169, reduced and standard tin) could reduce B^*_{c2} by ∼1 T [10]: perhaps acceptable for the current 12 T application, but likely to have a disproportionately larger impact on I_c for future accelerator magnets at 14 T and above. There is also evidence that a precipitous decrease in the irreversible strain limit is approached on reducing the heat treatment temperature to ∼640 °C for RRP® wires of the standard tin stoichiometry: for two 108/127 wires with 52–55 μm sub-element diameter (d_s), slightly smaller than ERMC-1, the acceptable window for heat treatment has been reported as (648 ± 3) °C or confined to ∼640 °C [11]. It was therefore decided to evaluate only reductions in duration, not temperature.

The results of stability tests for samples with this shorter heat treatment are shown in Fig. 6. The improvement in stability is striking, especially at 1.9 K: I_c could be measured without

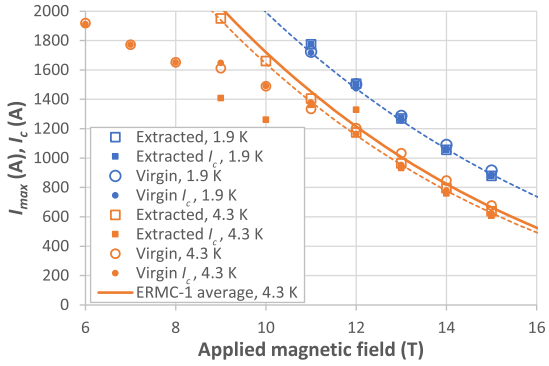

Fig. 6. Measured $I_{\max}(B)$ and $I_c(B)$ at 4.3 K and 1.9 K for virgin ERMC-1 wire and an extracted ERMC-1 strand from a trial ERMC cable after heat treatment with a shorter 30 h final plateau (650 °C 30 h). Dashed lines show the extrapolated $I_c(B)$ for the present samples; the solid line shows the extrapolated average virgin ERMC-1 wire $I_c(B)$ from wire acceptance tests at 4.3 K following the standard heat treatment for comparison.

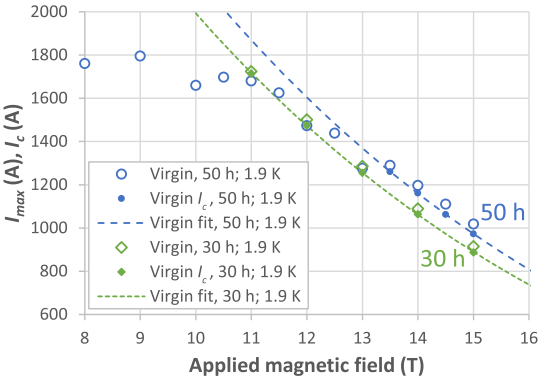

Fig. 7. Measured $I_{\max}(B)$ and $I_c(B)$ at 1.9 K for virgin ERMC-1 wire after 650 °C heat treatments with 30 h and 50 h final plateaus. Dashed lines show the extrapolated $I_c(B)$ for the present samples for each heat treatment.

quenches down to 11 T at both temperatures, and no cross-over between 1.9 K and 4.3 K performance is observed. Two points should, however, be noted: firstly, the shorter heat treatment results in some reduction in I_c, and secondly, the extracted strand reported here is from cable of the ERMC design, not FalconD (as discussed further in the next section).

The effect on I_c of the change in heat treatment is shown in Fig. 7; results are presented only at 1.9 K for clarity. At high fields for which a stable I_c could be measured in both cases (13.5–15 T), the 20 h reduction in heat treatment duration results in a reduction in I_c of 9%. The shorter heat treatment provides a net benefit for applications at 12 T and below: the I_c following the 30 h heat treatment matches or exceeds the quench current following the 50 h heat treatment in this range.

To assess the physical origins of this effect on stability and I_c, electron microscopy and RRR measurements were performed for round and rolled samples with different durations of the final heat treatment plateau. In Fig. 8, the RRR of samples with 30 h, 40 h and 50 h final steps are compared: for both round and rolled samples, there is a substantial increase in RRR of ~40% for the 40 h heat treatment and ~50% for the 30 h heat treatment, relative to the standard process.

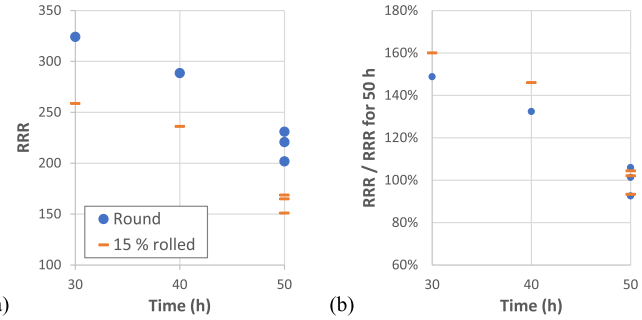

Fig. 8. (a) RRR and (b) RRR relative to that for the standard heat treatment for round (virgin) and 15% rolled ERMC-1 wire as a function of the duration of the final 650 °C plateau of the heat treatment.

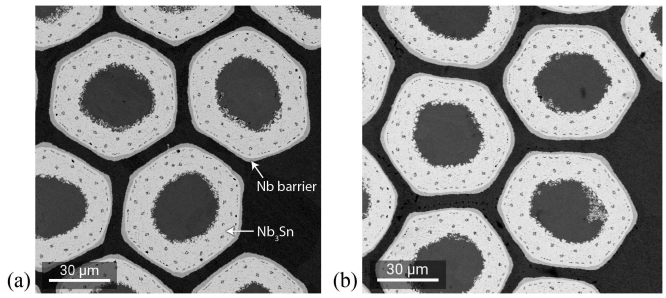

Fig. 9. Backscattered electron micrographs of ERMC-1 virgin wire samples reacted with a final step at 650 °C of (a) 30 h and (b) 50 h.

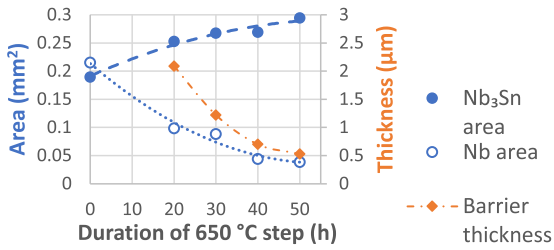

Fig. 10. Dependence on the duration of the 650 °C reaction step of the cross-sectional area of Nb and Nb_3Sn, and of the average unreacted Nb barrier thickness, for an ERMC-1 wire.

Image analysis was performed for backscattered electron micrographs of virgin wires quenched at selected times during the final heat treatment step (Fig. 9), from which the areas of Nb and Nb_3Sn, and the average residual unreacted thickness of the Nb barriers, were calculated (Fig. 10). The rate of Nb_3Sn formation decreases progressively: this is expected, as the growth rate is impacted both by the increasing thickness of the Nb_3Sn layers and the decreasing residual tin composition of the matrix, and the remaining unreacted Nb is increasingly confined to the barriers. The reduction in barrier thickness from 30–50 h is consistent with the reduction in RRR over this range, as tin lost across the barriers contaminates the copper matrix. The RRR deteriorates markedly after 40 h, but decreases by only ~10% between 30 h and 40 h. The rate of Nb_3Sn formation, on the other hand, decreases progressively with time: the area of Nb_3Sn increases

TABLE IV
CABLING DEGRADATION FOR EACH CABLE TYPE CONTAINING ERMC-1 WIRE, WITH MQXF CABLE FOR COMPARISON

Property	Cables of ERMC-1 Wire			MQXF
	FalconD		ERMC	
Keystone (°)	0.426	0.442	0	0.40
Pitch (mm)	110	120	120	109
I_c degradation, mean (%)	5.5	5.9	4.1	2.6
I_c degradation, range (%)	2.2–8.6	4.4–6.9	2.0–8.0	-
RRR, mean	202	206	228	-
RRR, range	175–232	176–244	189–265	-
RRR degradation, mean (%)	30.9	29.6	20.5	17

All results for the standard heat treatment of the wire type concerned (Table I). Cable types are defined in Table III.

only ∼3% from 40 h to 50 h. It is therefore likely that an optimum balance of I_c and RRR could be obtained in the 30–40 h range.

C. Cabling Degradation

The degradation of I_c and RRR on cabling is shown in Table IV for three trial cables of the FalconD and ERMC designs, and averaged over production for the MQXF cable for comparison, measured after standard heat treatments (Table I).

For the cables produced with the same strand type, it is clear that the degradation of both I_c and RRR is higher on average for the FalconD cable than for ERMC: this is consistent with the former being keystoned and having a lower mid-thickness, corresponding to a greater degree of compaction especially at the thin edge of the cable.

Relative to strand diameter, the MQXF cable has a slightly higher degree of compaction than FalconD, but a lower degradation of both I_c and RRR even than ERMC. This suggests a greater susceptibility to cabling degradation for the ERMC-1 wire. From the present data, it is not possible to distinguish whether this arises predominantly from differences between the 108/127 and 162/169 layouts (e.g., the substitution of superconducting sub-elements for copper near the wire center), or between reduced and standard tin stoichiometries.

D. Impact for Magnet Applications

For magnet applications, the required $I_c(B)$ and the impact of stability limitations on performance should be judged relative to the load line. In Fig. 11, the results of stability tests for virgin and extracted strands after both heat treatments (30 h and 50 h), and at both 1.9 K and 4.3 K, are collated in one plot and overlayed on the eRMC load line. As the quench currents do not drop below the intercept between $I_c(B)$ and the load line it would be expected that the self-field stability would be unproblematic in this application even for the standard 50 h heat treatment.

This should, however, be qualified: the plotted quench currents are average values from single samples (of each type) in a wire test configuration. The distributions of virgin strand characteristics and cabling degradation should be more fully sampled, and the differences in the strain state of the wire in operating conditions should also be considered.

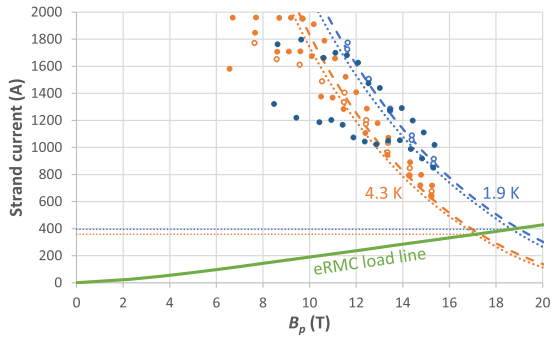

Fig. 11. eRMC load line scaled to the mean per-strand current, with the stability test results for both virgin and extracted strand sample of ERMC-1 reacted at 650 °C for 30 h (open markers) and 50 h (solid markers) superimposed. Data are plotted as a function of the magnetic field on the conductor (i.e., adjusted to include self-field).

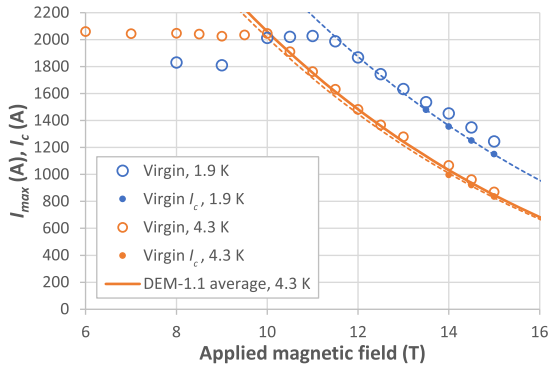

Fig. 12. Measured $I_{\max}(B)$ and $I_c(B)$ at 4.3 K and 1.9 K for virgin DEM-1.1 wire after the standard heat treatment (665 °C 50 h). Dashed lines show the extrapolated $I_c(B)$ for the present samples; the solid line shows the extrapolated average virgin DEM-1.1 wire $I_c(B)$ from wire acceptance tests at 4.3 K following the standard heat treatment for comparison.

VI. STABILITY OF DEM-1.1

A similar analysis was performed for the DEM-1.1 wire. This wire is identical to ERMC-1 in design, differing only in diameter. However, as a result of the larger sub-element size (and hence longer diffusion distances and thicker barriers), a standard heat treatment at the higher temperature of 665 °C was found to result in acceptable RRR.

The results of stability tests for virgin and extracted strands are shown in Figs. 12 and 13 respectively, where the extracted strand is from a trial cable with the R2D2 design. This cable is without core and keystone, with comparable compaction to the ERMC cable. As for ERMC-1, there is some cabling degradation, but for DEM-1.1 (and the R2D2 cable), the overall $I_{\max}(B)$ behavior is comparable for virgin and extracted strand: $I_{\max}(B)$ tracks the extrapolated $I_c(B)$ up to ∼2000 A (10 T and 11.5 T for 4.3 K and 1.9 K respectively). As ∼2000 A is the practical limit for current delivery for these sample holders, it is possible that the real quench currents at lower fields would be higher than plotted. There is nevertheless some indication that the quench current at 1.9 K drops below that at 4.3 K for magnetic fields of 9 T and below.

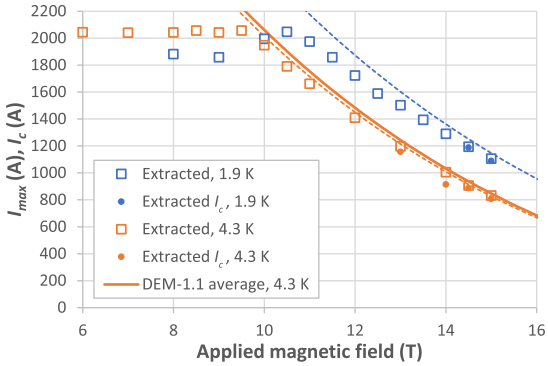

Fig. 13. Measured $I_{\max}(B)$ and $I_c(B)$ at 4.3 K and 1.9 K for an extracted DEM-1.1 strand from a trial R2D2 cable after the standard heat treatment (665 °C 50 h). The lines are virgin wire performance for comparison, as shown in Fig. 12.

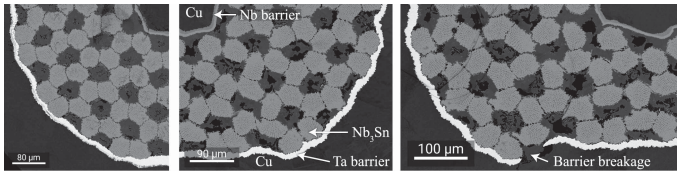

(a) Round (b) 15 % rolled (c) 30 % rolled

Fig. 14. SEM micrographs of reacted KAT Task 4 wire after rolling reductions of (a) 0% (round wire), (b) 15% and (c) 30%.

Applying the same alternative heat treatment investigated above for ERMC-1 – with a final plateau of 30 h at 650 °C – again has a stabilizing effect, allowing I_c at 1.9 K to be measured down to the lowest tested field of 12 T. Despite the fact that both the temperature and duration have been reduced relative to the standard heat treatment for this wire, I_c is reduced by a modest 4%; but B^*_{c2} (extrapolated from I_c measurements) is reduced by ∼0.5 T due to the temperature change, and overall stability behavior is unaffected, so there is little if any gain in quench currents.

VII. Cabling and Stability of KAT Wires

An earlier study of the deformation behavior of the 'Task 4' KAT wire found that the common diffusion barrier was intact for rolling reductions up to 15%, but showed local breakages at 30%, with undistorted Nb modules primarily sliding past each other on shear planes passing through tin cores (Fig. 14). In contrast, on cabling, in the most deformed edge sites, Nb modules show significant distortion.

In moving to Task 5, KAT successfully achieved long length production, with a mean piece length > 1.4 km, and introduced some small changes to the layout (e.g., a reduced Sn content, compensated by a revised heat treatment). Whilst this had some impact on the deformation behavior, the basic characteristics remain unchanged. For a trial cable in the FalconD design, strands near the center of the cable show very little distortion of Nb modules and the barrier remains intact, whilst strands in heavily deformed sites at the thin edge show local barrier breakages and module distortion (Fig. 15).

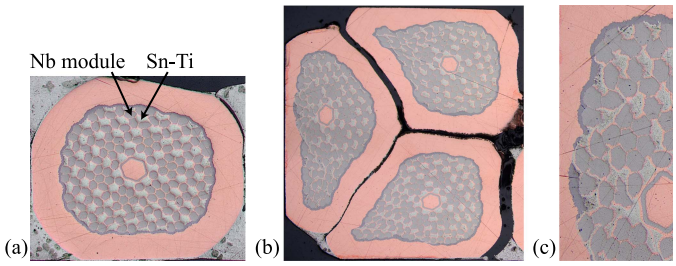

Fig. 15. Optical micrographs of unreacted KAT Task 5 wire after cabling in the R2D2 cable design: (a) Near the center of the cable, (b) at the thin edge, and (c) Enlargement of a region of (b) Showing barrier damage.

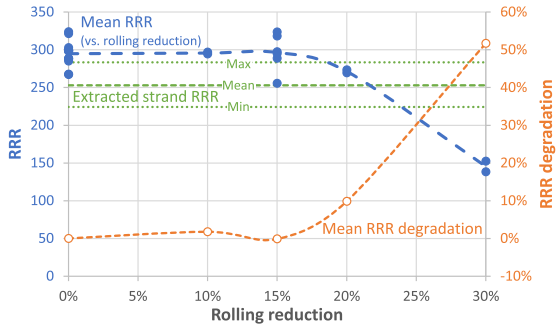

Fig. 16. RRR (blue, solid markers, left axis) and RRR degradation (orange, open markers, right axis) as a function of rolling reduction of KAT task 5 wires, with the range of extracted strand RRR (green) for comparison.

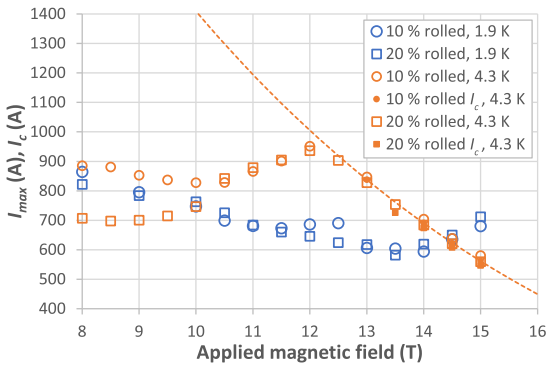

Fig. 17. Measured $I_{\max}(B)$ and $I_c(B)$ at 4.3 K and 1.9 K for KAT task 5 wire rolled with rolling reductions of 10% and 20%. The dashed lines show the extrapolated $I_c(B)$ at 4.3 K only.

Consistent with these observations, the average RRR of rolled wire with 15% reduction is comparable to that of round wire, with degradation beginning from a 20% rolling reduction (Fig. 16). The extracted strand RRR degradation does not exceed 30% and is half that on average – comparable to the RRP® examples, despite the barrier breakages.

Stability tests were performed for two rolled samples, with rolling reductions of 10% and 20% (Fig. 17). At 4.3 K, I_c could be measured down to 13 T, and the values for rolling reductions of 10% and 20% differed by <3%, suggesting the potential for low cabling degradation. However, the stability imposes a severe limitation on performance: at 1.9 K, all tests quenched, and the

quench current at 1.9 K is lower than the value at 4.3 K for applied magnetic fields as high as 14.5 T.

VIII. Discussion

The results of the stability tests of the RRP® wires are consistent with the starting premise – the self-field stability of the ERMC-1 and DEM-1.1 wires is poorer than that of the MQXF wire, due to their larger diameters, higher J_c and lower Cu/non-Cu fraction. Considering only round wire data, this would not be likely to limit magnet performance even for the standard heat treatments. But the high degradation of ERMC-1 – in stability as well as I_c and RRR – on cabling with the FalconD geometry highlights that J_c and diameter do not always dominate. As d_{eff} is not expected to drive self-field instabilities directly [5], [6], the poorer stability is more likely due to RRR degradation. The local RRR degradation at the thin edge has not yet been measured, but it will necessarily exceed the overall measured RRR degradation of ∼30.9% (Table IV): such values can exceed 50% [12], comparable to the changes observed in the heat treatment optimization study. Further study is needed to assess the relative contributions of the differences in design (Cu/non-Cu, d_{eff}, layout and stoichiometry) between the ERMC-1 and MQXF wires to the behavior on cabling.

Should improvements in stability be needed, it has been demonstrated that heat treatment optimization can deliver a significant improvement even for wires like ERMC-1 in which the parameter space is restricted by other considerations, and that there is potential for further optimizing the balance of I_c and RRR for durations in the 30–40 h range. It remains to be seen if this would also benefit extracted strand for the FalconD cable; and whether there is a gain in usable current depends on the load line for the application. It had previously been reported that there was little benefit in increasing RRR significantly beyond 100 [6], but that conclusion does not seem universal: in the present case, improved stability was found on increasing RRR ∼50% from an already high baseline of ∼200.

The higher J_c of ERMC-1 relative to the MQXF wire is due mostly to its larger sub-element size and the higher ('standard') Sn stoichiometry. The former may not be acceptable for future accelerator magnets [4], and the latter increasingly compromises RRR (or requires a low heat treatment temperature, compromising B^*_{c2} [10] and strain performance [11]) as the sub-element size is reduced [7]. It has not been tested specifically in the present study, but it is also likely that this contributes to higher local RRR degradation at cable edges than would be obtained for 'reduced tin' wires like MQXF. Heat treatment optimization to increase RRR or stability sacrifices a large part of the gain in J_c (relative to MQXF). It is therefore likely that the reduced tin formulation would be preferable in these applications, whilst also providing a larger parameter space for heat treatment optimization [11].

The contrast with the KAT Task 5 wire is again instructive. In this case the stability is unlikely to be acceptable for magnet applications without further improvement (it has not yet been tested whether heat treatment optimization is beneficial). As Nb modules do not have diffusion barriers, it is reasonable to expect that d_{eff} may exceed the geometrical size, especially after cabling deformation: magnetization data (not reported here) confirm it, and work is ongoing to improve the separation of the modules. But with the model of [6], the cause of poor *self-field* stability in 10% rolled samples is less clear: overall RRR is high, and microscopy does not suggest barrier breakages. In distributed tin wires after reaction, Nb_3Sn is separated from the Cu stabilizer by a significant length of resistive Cu-Sn, so there may be a need to reassess the impact of the conductivity gradients and stabilizer location.

Whilst the absence of sub-element diffusion barriers has disadvantages, and may impose a greater reliance on design optimization as heat treatment optimization is constrained by relatively longer diffusion distances, there are also promising signs for the potential of distributed tin designs. Geometrical sub-element sizes are already low, and could be reduced with less impact on Nb area than for distributed barrier designs; and for the cabling trial reported here, when the stability was sufficient to measure I_c, the cabling degradation was below 3%.

Indications of sensitivity to *local* degradation of RRR suggest there would be a significant added benefit in systematically measuring RRR locally at cable edges as well as the averaged value currently used at CERN.

Finally, it is important to note that only one sample of each type has been measured in the present study, and that tests by the *V–I* method alone cannot assess the full stability behavior (e.g., the effects of magnetization at lower field, or of perturbations of different energies). A fuller investigation is needed when evaluating new wire types in order to obtain statistics representative of the performance distribution of the wire. A previously reported approach using a laser to introduce perturbations with a precisely controlled energy [13] will be used to extend this analysis in future work.

IX. Conclusion

The cabling degradation and self-field stability of three RRP® and distributed tin wires of ≥1 mm diameter have been evaluated and compared to a reference 0.85 mm RRP® wire.

The ≥1 mm diameter RRP® 162/169 wires show quenches below the extrapolated critical current at intermediate magnetic fields, especially for strands of the ERMC-1 (1.0 mm) wire extracted from relatively highly compacted cables. It has, however, been demonstrated that heat treatment optimization can be effective to improve stability, increasing RRR for a modest reduction in I_c, even when the starting value of RRR is high (∼200); and for an appropriate choice of heat treatment, the results indicate adequate self-field stability for the foreseen applications, including eRMC and R2D2. Considerations for the future selection of RRP® wires have also been discussed.

The KAT distributed tin wire has comparable J_c to the reference MQXF RRP® wire, and good potential for combining small sub-element size and high J_c. The results of this study show promising indications of low cabling degradation, but much poorer stability. Further development is in progress to understand the causes of the instability and address them in the wire design and heat treatment.

ACKNOWLEDGMENT

The authors would like to thank Kiswire Advance Technology (KAT) for development of the distributed tin conductors, Emma Gautheron for providing the eRMC load line, and all their colleagues in TE-MSC-SCD (CERN) involved in the cabling and testing, including Angelo Bonasia, Pierre-François Jacquot and Anne Eychenne.

REFERENCES

[1] A. Ballarino and A. Devred, *The MSC HFM Activities: Strategies and Milestones – Part 1: Nb_3Sn*. Meyrin, Geneva, Switzerland: CERN, 2022. [Online]. Available: https://edms.cern.ch/document/2680109

[2] A. Pampaloni et al., "Mechanical design of FalconD, a Nb$_3$Sn cosθ short model dipole for the FCC," *IEEE Trans. Appl. Supercond.*, vol. 32, no. 6, Sep. 2022, Art. no. 4000605.

[3] V. Calvelli et al., "R2D2, the CEA graded Nb$_3$Sn research racetrack dipole demonstrator magnet," *IEEE Trans. Appl. Supercond.*, vol. 31, no. 5, Aug. 2021, Art. no. 4002706.

[4] A. Ballarino and L. Bottura, "Targets for R&D on Nb$_3$Sn conductor for high energy physics," *IEEE Trans. Appl. Supercond.*, vol. 25, no. 3, Jun. 2015, Art. no. 6000906.

[5] M. Wilson, *Superconducting Magnets*. Oxford, U.K.: Clarendon, 1983.

[6] B. Bordini, L. Bottura, L. Oberli, L. Rossi, and E. Takala, "Impact of the residual resistivity ratio on the stability of Nb$_3$Sn magnets," *IEEE Trans. Appl. Supercond.*, vol. 22, no. 3, Jun. 2012, Art. no. 4705804.

[7] M. B. Field, Y. Zhang, H. Miao, M. Gerace, and J. A. Parrell, "Optimizing Nb$_3$Sn conductors for high field applications," *IEEE Trans. Appl. Supercond.*, vol. 24, no. 3, Jun. 2014, Art. no. 6001105.

[8] S. Izquierdo Bermudez, R. Ortwein, J. C. Perez, and E. Rochepault, "Design of ERMC and RMM, the base of the Nb$_3$Sn 16 T magnet development at CERN," *IEEE Trans. Appl. Supercond.*, vol. 27, no. 4, Jun. 2017, Art. no. 4002004.

[9] A. K. Ghosh et al., "Dynamic stability threshold in high-performance internal-tin Nb$_3$Sn superconductors for high field magnets," *Supercond. Sci. Technol.*, vol. 18, no. 1, pp. L5–L8, Jan. 2005.

[10] L. D. Cooley, A. K. Ghosh, D. R. Dietderich, and I. Pong, "Conductor specification and validation for high-luminosity LHC quadrupole magnets," *IEEE Trans. Appl. Supercond.*, vol. 27, no. 4, Jun. 2017, Art. no. 6000505.

[11] N. Cheggour, T. C. Stauffer, W. Starch, L. F. Goodrich, and J. D. Splett, "Implications of the strain irreversibility cliff on the fabrication of particle-accelerator magnets made of restacked-rod-process Nb$_3$Sn wires," *Sci. Rep.*, vol. 9, no. 1, 2019, Art. no. 5466.

[12] M. D. Sumption et al., "Effect of cable edge deformation on RRR and magnetization of strands extracted from Nb$_3$Sn Rutherford-type cables," *IEEE Trans. Appl. Supercond.*, vol. 19, no. 3, pp. 2481–2485, Jun. 2009.

[13] E. Takala, B. Bordini, J. Bremer, C. Balle, L. Bottura, and L. Rossi, "An experimental setup to measure the minimum trigger energy for magnetothermal instability in Nb$_3$Sn strands," *IEEE Trans. Appl. Supercond.*, vol. 22, no. 3, Jun. 2012, Art. no. 6000704.